doi.org/10.21640/ns.v12i24.2152
Sección: Ciencias Naturales e Ingenierías

Segmentación de imágenes de cultivos utilizando descriptores morfológicos adaptativos

Crop Images Segmentation using Adaptive Morphologic Descriptors

Miguel Ángel Gil Rios[1, 2]
Juan Manuel López Hernández[2]
Dolores Juárez Ramírez[1]
María del Carmen Ruiz Robledo[1]
Laura Paulina Badillo Canchola[1]
Ariana Aranda López[1]

[1] Universidad Tecnológica de León, Tecnologías de la Información y Comunicación
[2] Universidad de Guanajuato, División de Ciencias e Ingenierías, Yuriria

Autor para correspondencia: Miguel Ángel Gil Rios, E-mail: angel.grios@gmail.com

Resumen

Esta investigación está enfocada en mejorar los resultados de segmentación de imágenes de cultivos mediante el uso de descriptores morfológicos adaptativos, en lugar de algoritmos clásicos o el uso del operador top-hat utilizando descriptores morfológicos predefinidos como el disco y el diamante. Una de las técnicas más utilizadas para la segmentación de imágenes de cultivos es el algoritmo K-Means. Sin embargo, este algoritmo tiene el inconveniente de llegar a diferentes resultados de segmentación en la misma imagen, dada su inicialización aleatoria. Adicionalmente, el tiempo requerido para segmentar imágenes de tamaño considerable, como lo son las fotografías de cultivos adquiridas principalmente mediante drones, es significativo. Los resultados obtenidos con la técnica propuesta son comparados contra los obtenidos por el algoritmo K-Means así como los resultados que se obtuvieron al utilizar descriptores morfológicos con formas predeterminadas de la literatura.

Palabras clave: segmentación de imagen; descriptor morfológico; detección de cultivos; UMDA

Introducción

La segmentación de imágenes digitales por medio de la computadora es una de las tareas más difíciles ya que, factores como el ruido dentro de la imagen, nitidez, contraste y forma irregular de los objetos influyen significativamente en los resultados que se obtienen. En la literatura actual se pueden encontrar diversos métodos para la segmentación de imágenes. Por ejemplo, para la detección de arterias, existen métodos que tratan de aproximar la forma de las arterias a estructuras tubulares, las cuales son rotadas durante el proceso de detección. Otros métodos, utilizan los eigenvalores obtenidos de la segunda derivada de una función gaussiana con el fin de obtener una métrica que permita clasificar los pixeles que forman parte de las arterias de aquellos que conforman el resto de la imagen (Frangi, 1998; Wang, 2012). Aun cuando las técnicas como la anterior han dado resultados óptimos, no ha sido así en la segmentación de imágenes de cultivos debido a que es muy difícil aproximar las formas de los cultivos a estructuras tubulares o curvas continuas. Por tal motivo, el algoritmo K-Means se ha utilizado ampliamente para dicho fin (Jaware, 2012, 190; Patil, 2016). Adicionalmente, existe otra técnica de segmentación de imágenes, la cual está basada en el concepto de morfología matemática (Eiho, 1997, p. 696). La segmentación de imágenes utilizando morfología matemática hace uso de descriptores morfológicos, también llamados elementos estructurantes, los cuales están definidos por medio de forma y tamaño, haciendo a su vez, uso de un operador denominado top-hat. Actualmente, esta técnica es ampliamente utilizada y, elementos estructurantes como el disco y el diamante son utilizados ampliamente, obteniendo resultados satisfactorios. Sin embargo, en la segmentación de imágenes de cultivos, los resultados han podido mejorarse al utilizar elementos estructurantes adaptativos en lugar de las formas clásicas como el disco y el diamante. Los elementos estructurantes adaptativos se generan utilizando el Algoritmo de Distribución Marginal Univariado conocido por sus siglas en inglés como UMDA (Guerrero-Turrubiates, 2017, p. 1; Hauschild, 2011, p. 111). Los resultados obtenidos al aplicar esta técnica son mejores que utilizando el algoritmo K-Means así como la misma morfología matemática cuando se emplean las formas clásicas de disco y rombo, tal y como se describe en la sección de resultados y discusión.

Abstract

This research is focused on the segmentation improvement of crop images by using adaptive morphologic descriptors instead of classic algorithms like K-means and the top-hat operator using predefined shapes like disk or diamond. Obtained results shows that using an adaptive morphologic descriptor improves the segmentation performance against the classic shapes like disc and diamond. In order to measure the process a set of 60 crop images was used including their respective ground-truth images. The images were segmented using the K-Means algorithm and the top-hat operator with the disk and diamond shapes at different sizes into a range to validate their performance. In order to generate the adaptive morphologic descriptor, the Univariated Marginal Distribution Algorithm was used with no constraints by exploring a range of different sizes. Also, performance metrics like receiver operating characteristic and accuracy rate were applied to the generated data in order to assess the results.
Keywords: image segmentation; morphologic descriptor; crop detection; UMDA

Recibido en: 28-09-2019
Aceptado en: 29-01-2020

Introduction

Automated image segmentation to detect domain-specific objects and elements is a challenging task in the image processing field because of high noise levels, low contrast and non-regular object shapes. Most state of the art methods segment images applying techniques focused into find predefined forms close to the shape of the searched objects. For example, for vessels detection in angiographic images, some methods try to approximate retinal arteries as tubular structures that are rotated at different orientations on the process. Other methods use the eigenvalues of a second order derivative of a Gaussian function in order to compute a vesselness measure to classify the vessel-like structures (Frangi, 1998; Wang, 2012). Due of the second derivative, detection process is highly sensitive to noise into the image. Even though the previous techniques has proven achieve good results, they are not optimal for crop detection since it is

difficult to approximate crop shapes as tubular structures or continuos curves. For that reason, K-Means has been used widely into the crop image segmentation field (Jaware, 2012, p. 190; Patil, 2016). However, there exists other technique to segment images based on a concept called mathematical morphology. That method was proposed by Eiho and Qian and is widely used since it is governed by the parameters of size and shape of a structuring element (SE) (Eiho 1997, 696). This method uses the top-hat operator to enhance certain structures. Actually, the technique is well-known and canonical structuring elements like disk or rhombus are widely used. Due to the use of top-hat operator, this method has proved achieve good results in coronary vessels detection (Bouraoui, 2008, p. 1059; Sun and Sang, 2008). Also, performance and effectiviness of the original technique can be improved by using stochastic strategies like Genetic Algorithms (GAs) or Estimation of Distribution Algorithms (EDAs) (Cruz, 2015, p. 297; Guerrero-Turrubiates 2017, p. 1; Hauschild, 2011, p. 111). The morphological top-hat operator achieves a suitable performance for enhancing specific-domain objects; however, the process to determine the size and shape of the SE involves a trial-and-error stage or a selection based on an expert knowledge. To overcome the a-priori knowledge about the form and shape of the structuring element, an evolutive morphological descriptor is used in order to obtain a highly accurate SE by introducing the Univariate Marginal Distribution Algorithm (UMDA) for its design and the obtained results are better than K-Means technique and the Top-Hat operator using canonical shapes like disc and rhombus.

Method

Image Dataset. To measure the SE performance of the proposed method the crop-weed dataset was used. It contains a set of 60 crop image files with their respective ground-truth images (Haugh 2015, 105).

K-Means. The K-Means algorithm is a widely known unsupervised classification algorithm. It was proposed in 1967 by MacQueen (MacQueen, 1967). This technique requires a-priori to know the *k* value since it represents the number of clusters or classes to be formed by the process. On

the successive steps, the technique initializes randomly *k* points that will be moved by an iterative process in order to form the final clusters automatically as described in Algorithm 1.

Algorithm 1 K-Means Algorithm	
Require: *k* = number of clusters to be formed	
	Initialize *k-points* (called means) randomly **repeat** 1. re(assign) each object to the closest *centroid* 2. Update the cluster means, i.e, calculate the mean value of the objects for each cluster **until no change**

Fig. 1 shows an example of the classes (clusters) found by K-Means algorithm.

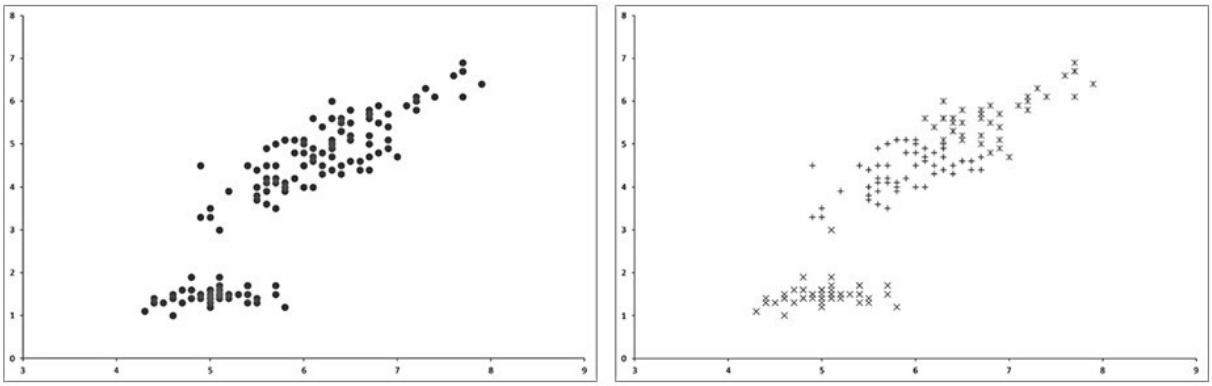

Fig. 1. Example of clusters formed by K-Means using *k=3*. On the left side the original dataset is represented. The right side shows the clustered data by the K-Means algorithm.

Main advantage of K-Means relies in the automatic classification made by an iterative process starting from several initial points called centroids wich are placed randomly across the data space and after moved or reallocated to their respective new clusters centers after each iteration. The process ends when centroids are not moved anymore. Although the algorithm is easy to implement, it could achieve to different classification results with the same data because of its stochastic centroids initialization.

Morphological top-hat operator. The morphological top-hat operator (Meyer, 1977) for grayscale images is part of the basic toolbox of mathematical morphology operators (Soille, 1999). Its function is to detect contrasted objects on non-uniform backgrounds. For grayscale images, there are two versions: the white top-hat which extracts bright structures and the black top-hat extracts dark structures. White top-hat operator is defined as the difference between an input image *f* and its opening as stated in equation (1).

$$\boldsymbol{\rho(f) = f - \gamma(f)} \quad (1)$$

Where γ(f) denotes the opening operation.

On this research, the white top-hat was used since crops tends to be brighter than their surroundings and in addition, it corrects nonuniform lighting condition and make obvious contrast between background and objects. The performance of the top-hat operator depends on two factors: the shape and the size of the structuring element that is used. Fig. 2 shows a crop image with their corresponding ground-truth image outlined by a specialist on first column. Remaining columns shows the response of the top-hat operator using different shapes and sizes.

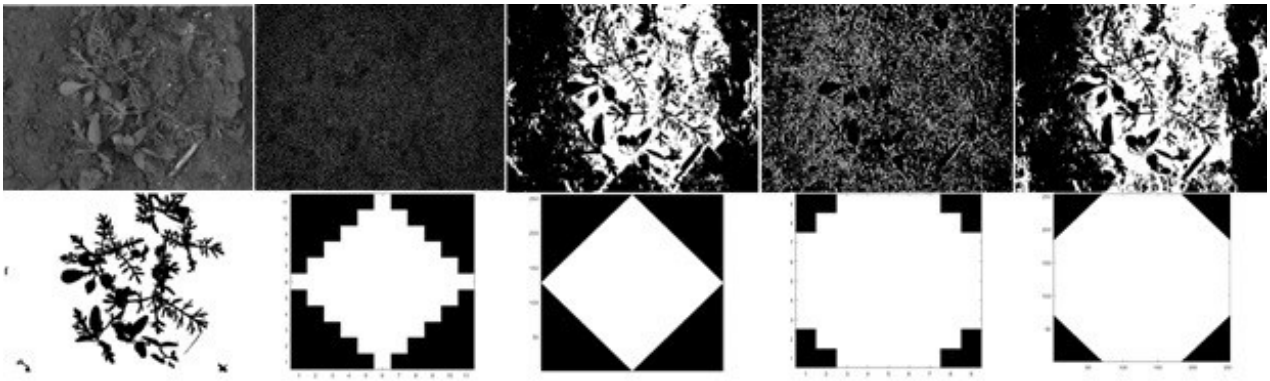

Fig. 2. First column: Original crop image on first row and their corresponding ground-truth on second row. **Second column:** On first row, the top-hat response; on second row the diamond shape (with size = 5) used as structuring element. **Third column:** On first row, the top-hat response; on second row, the diamond shape (with size=127) used as structuring element. **Fourth column:** On first row, the top-hat response; on second row, the disk shape (with size=5) used as structuring element. **Fifth column:** On first row, the top-hat response; on second row, the disk shape (with size=127) used as structuring element. For purposes of better visualization, contrast was improved on images placed in first row from columns 2 to 5.

Univariate Marginal Distribution Algoritm. UMDA is a population technique-based like Genetic Algorithms (GA) (Heinz, 2001, p. 135). Instead of the population recombination and mutation concepts, UMDA use the frequency of components in a population of candidate solutions in the construction of new candidate solutions. Each individual in the population is formed by a bit-string and it is denoted as: $\boldsymbol{x_i} = [x_{i,1}, x_{i,2}, \dots, . x_{i,D}]$ and each element $x_{i,j}$ is called a gene. An array of vectors $X = \left[x_1, x_2, \dots, x_{n_{pop}}\right]$ is called a population. On this approach, the

population evolves on each generation (iteration) t and the current population is denoted as X^t. On each iteration UMDA samples a subset $n_{set}$with the individuals representing the best solutions. With the n_{set} sample a new population (generation) is created based on a probabilistic model using the genes in the individuals. This iterative process ends when an error criterion is accomplished, or a maximum value of generations is reached. Unlike other population-based techniques, UMDA only requires three parameters to operate: population size, stopping criterion and population selection ratio. UMDA pseudocode is described in Algorithm 2.

Algorithm 2 Univariate Marginal Distribution Algorithm

Require: D = dimensions of the problem

n_{pop} = Population size
N_{gen} = Number of maximum generations
n_{sel} = Selected set size
Initialize $t = 0, X^t \sim U(0,1)$
Evaluate $F^t = f(X^t)$
$[x_{best}, X^t] = sort\ X^t$ according to objective values
while stop_criterion ≠ **true do**
  for i = 1...D **do**
    $p_i = \sum_j^{n_{sel}} x_{i,j}$
  end for
  Set $P = [p_1, p_2, \dots, p_D]$
  Sample $X^{t+1} \sim P$
  Elitism $X^{t+1} = \left[X_{1:(n_{pop}-1)}^{t+1},\ x_{best}\right]$
  $t = t + 1$
  Evaluate $F^t = f(X^t)$
  $[x_{best}, X^t] = Sort\ X^t$ according to objective values
end while
return x_{best}

Adaptive Morphological Descriptor. Based on the methods described above, a morphologic descriptor is generated in the form of a structuring element (SE) that is used with the top-hat operator in order to segment crop images. Main advantage of this approach relies in the construction of a SE based on the crop image features rather than a predefined or empirical shape. This method is focused in the generation of the best suitable SE by exploring the search space delimited by its size and finding the best pixels distribution along them. Also, the UMDA is used with a wide range of SE sizes to determine the best suitable morphologic descriptor avoiding an empirical trial and error procedure. Using this approach, the method can find and determine the

shape and size of the SE in an automated way. In Fig. 3, six different SE's generated by UMDA are presented.

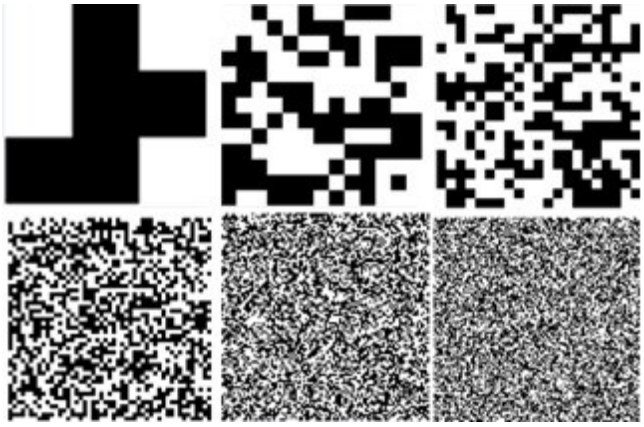

Fig. 3. Six different structuring elements generated by the UMDA. Sizes in pixels from left to right and up to down: 3x3, 13x13, 23x23, 49x49, 96x96 and 127x127.

Thresholding Otsu Method

Thresholding is an important technique in image segmentation applications. The basic idea of thresholding is to select an optimal gray-level threshold value for separating objects of interest in an image from the background based on their gray-level distribution. While humans can easily differentiable an object from complex background and image thresholding is a difficult task to separate them (Vala, 2013). Otsu method is type of global thresholding in which it depends only gray value of the image. Otsu method was proposed by Scholar Otsu in 1979. Otsu method is global thresholding selection method, which is widely used because it is simple and effective (Qu, 2010). The Otsu method requires computing a gray level histogram before running. However, because of the one-dimensional which only consider the gray-level information, it does not give better segmentation result. So, for that two-dimensional Otsu algorithms was proposed which works on both gray-level threshold of each pixel as well as its Spatial correlation information within the neighborhood. For that reason, Otsu algorithm can obtain satisfactory segmentation results when it is applied to the noisy images (Jian-zhuang 1991).

Once the image was segmented by using the top-hat operator a thresholding process is necessary in order to classify in a deterministic way those pixels belonging to conform crops from those that does not.

Evaluation Metrics

In order to asses the performance of the proposed method and select the best SE achieved by it, the receiver operating characteristic (ROC) curve graph and measures of sensitivity, specificity and accuracy were used (Zhu 2010). Also, the True-Positive Rate (FPR), True-Negative Rate (TNR), False-Positive Rate (FPR) and False-Negative Rate (FNR) metrics are used to measure the classifiers performance.

The TPR represents the fraction of elements that are positives and the classifier mark them as positives. The TNR represents the fraction of elements that are negatives and the classifier mark them as negatives. The FPR represent the fraction of elements that are negatives and the classifier mark them as positives. Fnially, the FNR represent the fraction of elements that are positives and the classifier mark them as negatives.

For this research the TPR represents the fraction of the crop pixels outlined by the specialist that are correctly detected by the method. The false-positive rate (FPR) is used to measure the proportion of actual negatives (non-crop pixels) that are incorrectly classified as positives (crop pixels). The TPR along the SE size provides information about how the SE shape and size is related with its performance to detect positive crops pixels.

By using TPR and FNR factors, the Sensitivity measure can be calculated by applying Eq. (2).

$$Sensitivity = \frac{TPR}{TPR + FNR} \tag{2}$$

Eq. (3) is used to measure the the Specificity, which represents the non-crop pixels (background pixels) that are correctly detected as such by the method.

$$Specificity = \frac{TNR}{TNR + FPR} \quad (3)$$

Accuracy represents the fraction of crop and non-crop pixels correctly detected by the method and is the most used measure to evaluate binary classification, which is defined in Eq.(4).

$$Accuracy = \frac{TPR + TNR}{TPR + FPR + TNR + FNR}, \quad (4)$$

Where *TPR* and *TNR* represent the fractions of crop and non-crop pixels correctly segmented, and *FPR* and *FNR* the fractions of incorrectly classified pixels.

ROC graphs are another way besides confusion matrices to examine the performance of classifiers (Swets 1988, 1285). A ROC graph is a plot with the false positive rate on the *x-axis* and the true positive rate on the *y-axis*. The point (0,1) is the perfect classifier: it classifies all positive cases and negative cases correctly. It is (0,1) because the FPR is 0 (none), and the TPR is 1 (all). The point (0,0) represents a classifier that predicts all cases to be negative, while the point (1,1) corresponds to a classifier that predicts every case to be positive. Point (1,0) is the classifier that is incorrect for all classifications. In many cases, a classifier has a parameter that can be adjusted to increase TPR at the cost of an increased FPR or decrease FPR at the cost of a decrease in TPR. Each parameter setting provides a (FPR, TPR) pair and a series of such pairs can be used to plot a ROC curve. A non-parametric classifier is represented by a single ROC point, corresponding to its (FPR, TPR) pair.

Experiment

Since the top-hat operator is governed by the size and shape of the SE, a wide range of sizes were used on the performed tests starting with a 1x1 up to 127x127 pixels. In order to measure how the shape of an auto-generated SE influences the result, the UMDA was performed 30 times on each

test image selecting the best achieved solution for each of them. The UMDA parameters were set as: 30 individuals, 30 generations and a selection rate of 0.70. The number of genes for each individual was set on 1, 9, 25, …, 16129, as each test was varying the SE size beginning with a size of 1x1 and finishing with a size of 127x127. These values were determined according to the best tradeoff between detection performance and computational time (Alba, 2006, p. 242; Cruz, 2015, p. 297; Hisashi, 2003, p. 112; Marler, 2010, p. 853; Topon, 2003, p. 1259). The final black and white image was obtained using the Otsu method. To assess the obtained results, the corresponding ground-truth for each test image was used. Ground-truth images are created from their corresponding originals and outlined by specialists. Since main goal of automated computing processing is trying to emulate human intelligence, the ground-truth elements provide an initial base to compare results obtained by automated computing algorithms. However, there does not exists a unique "truth" since two different human experts can achieve different results for the same problem or element. In the process of attempting to evaluate several recognition algorithms an uncovered number of serious hurdles with the ground-truthing elements are present. This problem may, in fact, be much more dificult than it appears. Ground-truthing is so hard, including the notions that there may exist more than one acceptable "truth" and/or incomplete or partial "truths" (Hu, 2001). Even though expert outlined ground-truth images could not represent a complete "truth", they provide an initial base to measure automated computing results. This is the main reason why the ground-truth images provided by the dataset were used to assess the results.

The tests were performed over an Intel i7-4770 processor at 3.40 GZ with 8GB of RAM. All the tests were programmed on Matlab. The mentioned hardware and software was provided by the Universidad Tecnológica de León.

Results

After tests execution important results were obtained, and they are explained on this section.

The performance results obtained for each image segmentation using the SE's generated by UMDA are described in Table 1.

Table 1. Performance results obtained for each segmented image using the SE's generated by UMDA.

File	Accuracy	TPR	TNR	FPR	FNR
001_Image.png	0.9445	0.7590	0.9843	0.0157	0.2410
002_Image.png	0.9424	0.7865	0.9624	0.0376	0.2135
003_Image.png	0.9495	0.7992	0.9631	0.0369	0.2008
004_Image.png	0.9518	0.8005	0.9712	0.0288	0.1995
005_Image.png	0.8338	0.8728	0.8314	0.1686	0.1272
006_Image.png	0.9632	0.7421	0.9879	0.0121	0.2579
007_Image.png	0.9486	0.7708	0.9830	0.0170	0.2292
008_Image.png	0.9446	0.7581	0.9644	0.0356	0.2419
009_Image.png	0.9607	0.8120	0.9749	0.0251	0.1880
010_Image.png	0.9509	0.8358	0.9593	0.0407	0.1642
011_Image.png	0.9510	0.7853	0.9641	0.0359	0.2147
012_Image.png	0.7952	0.9574	0.7899	0.2101	0.0426
013_Image.png	0.9484	0.7597	0.9647	0.0353	0.2403
014_Image.png	0.9515	0.8745	0.9550	0.0450	0.1255
015_Image.png	0.8608	0.7804	0.8660	0.1340	0.2196
016_Image.png	0.9472	0.7867	0.9625	0.0375	0.2133
017_Image.png	0.9558	0.8029	0.9641	0.0359	0.1971
018_Image.png	0.9553	0.7746	0.9711	0.0289	0.2254
019_Image.png	0.8437	0.8903	0.8416	0.1584	0.1097
020_Image.png	0.7456	0.9428	0.7421	0.2579	0.0572
021_Image.png	0.8131	0.8900	0.8113	0.1887	0.1100
022_Image.png	0.9447	0.8023	0.9536	0.0464	0.1977
023_Image.png	0.9673	0.7874	0.9805	0.0195	0.2126
024_Image.png	0.9686	0.8111	0.9784	0.0216	0.1889
025_Image.png	0.9125	0.8505	0.9170	0.0830	0.1495
026_Image.png	0.9499	0.6633	0.9648	0.0352	0.3367
027_Image.png	0.9351	0.8163	0.9444	0.0556	0.1837
028_Image.png	0.9519	0.7575	0.9760	0.0240	0.2425
029_Image.png	0.9324	0.7422	0.9775	0.0225	0.2578
030_Image.png	0.8057	0.9448	0.8025	0.1975	0.0552
031_Image.png	0.9075	0.5584	0.9639	0.0361	0.4416
032_Image.png	0.9464	0.7941	0.9630	0.0370	0.2059
033_Image.png	0.9606	0.7840	0.9775	0.0225	0.2160
034_Image.png	0.9540	0.7703	0.9761	0.0239	0.2297
035_Image.png	0.9410	0.7553	0.9562	0.0438	0.2447
036_Image.png	0.9470	0.7093	0.9808	0.0192	0.2907
037_Image.png	0.8675	0.8861	0.8667	0.1333	0.1139
038_Image.png	0.9340	0.7390	0.9620	0.0380	0.2610
039_Image.png	0.8688	0.8489	0.8695	0.1305	0.1511
040_Image.png	0.9141	0.6601	0.9487	0.0513	0.3399
041_Image.png	0.9642	0.8056	0.9732	0.0268	0.1944
042_Image.png	0.9627	0.8078	0.9698	0.0302	0.1922
043_Image.png	0.8842	0.8911	0.8840	0.1160	0.1089
044_Image.png	0.9731	0.7626	0.9797	0.0203	0.2374
045_Image.png	0.9597	0.7823	0.9742	0.0258	0.2177
046_Image.png	0.9792	0.8663	0.9820	0.0180	0.1337
047_Image.png	0.9446	0.8329	0.9483	0.0517	0.1671
048_Image.png	0.9340	0.8443	0.9378	0.0622	0.1557
049_Image.png	0.9585	0.7636	0.9661	0.0339	0.2364
050_Image.png	0.7643	0.9525	0.7612	0.2388	0.0475
051_Image.png	0.9534	0.7643	0.9871	0.0129	0.2357
052_Image.png	0.9475	0.8136	0.9648	0.0352	0.1864
053_Image.png	0.9085	0.7174	0.9206	0.0794	0.2826
054_Image.png	0.9637	0.8040	0.9830	0.0170	0.1960
055_Image.png	0.9584	0.8197	0.9732	0.0268	0.1803
056_Image.png	0.9464	0.7746	0.9691	0.0309	0.2254
057_Image.png	0.9413	0.7808	0.9604	0.0396	0.2192
058_Image.png	0.9443	0.7848	0.9718	0.0282	0.2152
059_Image.png	0.9487	0.8020	0.9677	0.0323	0.1980

060_Image.png	0.9648	0.7965	0.9857	0.0143	0.2035

In Table 2, is presented a summarized set of records containing the calculations of TPR and FPR that conforms the ROC for the two classic and the adaptive SE. Table rows were summarized to present the most significant SE sizes were the curve changes their behavior and takes their final stability.

Table 2. Summary of TPR and FPR calculations for the disk, diamond and autogenerated SE shapes. Summary was formed with the first 5 records containing SE size in a range from 1 to 9, second set of 5 rows contains SE size in a range from 65 to 73 and, last set of 5 rows contains SE size from 119 to 127.

	Disc			Diamond			Adaptive		
SE Size	**Accuracy**	**TPR**	**FPR**	**Accuracy**	**TPR**	**FPR**	**Accuracy**	**TPR**	**FPR**
1	0.7625	0.1922	0.1875	0.7625	0.1922	0.1875	0.9198	0.0000	0.0000
3	0.8101	0.2393	0.1387	0.8191	0.2362	0.1283	0.8000	0.1570	0.1437
5	0.8663	0.2547	0.0782	0.8716	0.2641	0.0730	0.8308	0.2017	0.1135
7	0.8902	0.3481	0.0596	0.8875	0.3299	0.0611	0.8604	0.2324	0.0827
9	0.8991	0.4109	0.0554	0.8974	0.3934	0.0557	0.8799	0.2722	0.0647
65	0.9098	0.8319	0.0790	0.9145	0.8276	0.0737	0.9261	0.8005	0.0594
67	0.9079	0.8321	0.0810	0.9135	0.8286	0.0749	0.9253	0.8050	0.0607
69	0.9084	0.8328	0.0804	0.9121	0.8287	0.0763	0.9253	0.8068	0.0609
71	0.9077	0.8331	0.0813	0.9110	0.8295	0.0775	0.9240	0.8115	0.0625
73	0.9074	0.8342	0.0817	0.9111	0.8300	0.0774	0.9232	0.8133	0.0635
119	0.9033	0.8304	0.0853	0.9053	0.8322	0.0837	0.9116	0.8322	0.0771
121	0.9047	0.8294	0.0838	0.9046	0.8323	0.0843	0.9116	0.8335	0.0774
123	0.9035	0.8301	0.0851	0.9038	0.8322	0.0850	0.9108	0.8347	0.0783
125	0.9043	0.8302	0.0843	0.9029	0.8315	0.0860	0.9105	0.8340	0.0785
127	0.9040	0.8297	0.0846	0.9028	0.8314	0.0860	0.9101	0.8345	0.0790

Fig. 4 shows the performance averages for the accuracy and the SE size in a range from 1 to 127.

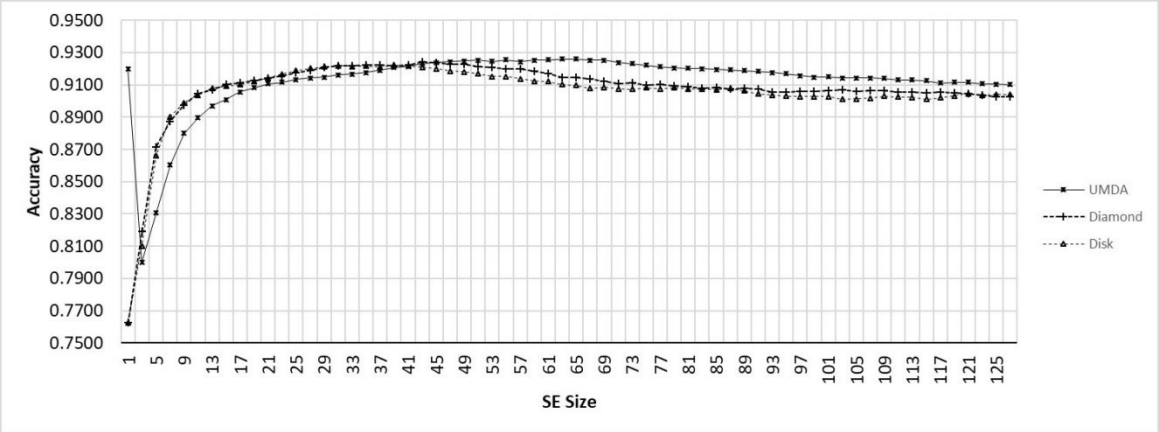

Fig. 4. Performance of different SE sizes, from *1x1* to *127x127* (*x-axis*) and Accuracy mean (*y-axis*).

In Fig. 5 the performance for each shape is presented separately.

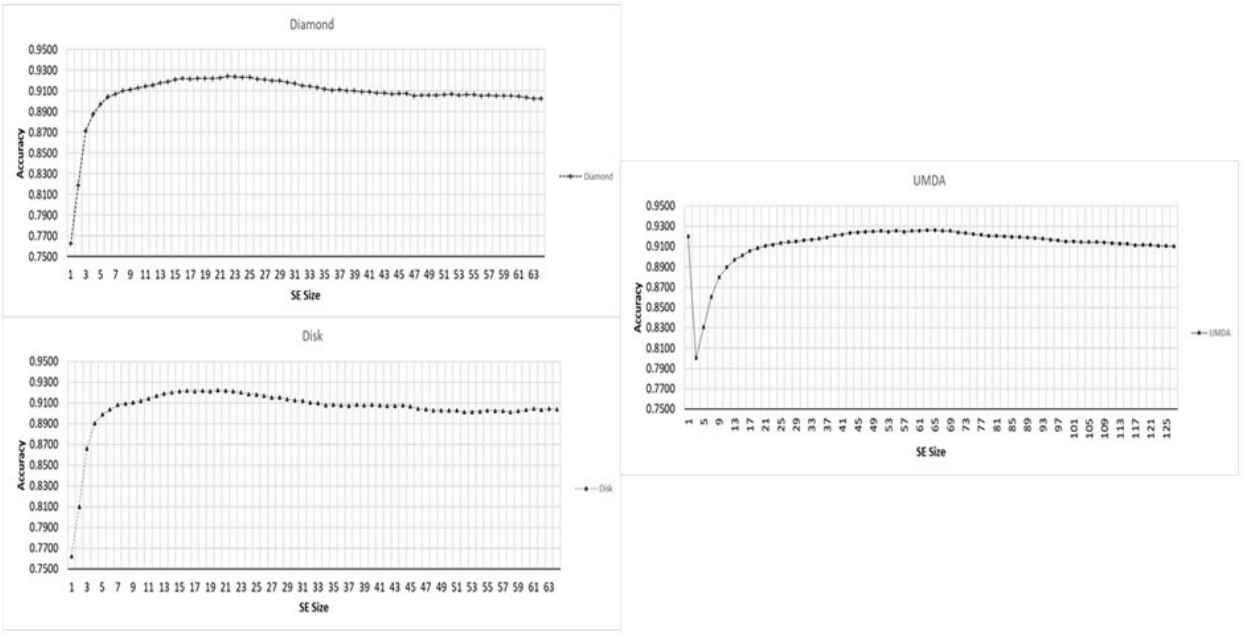

Fig. 5. Performance for different SE sizes, from *1x1* to *127x127* (*x-axis*) and Accuracy mean (*y-axis*) for each shape type.

In Fig. 6 the ROC curve is shown in order to know the best structuring SE size by contrasting TPR and FPR factors for different types of SE's. The studied parameter to measure the classifier performance was the SE size.

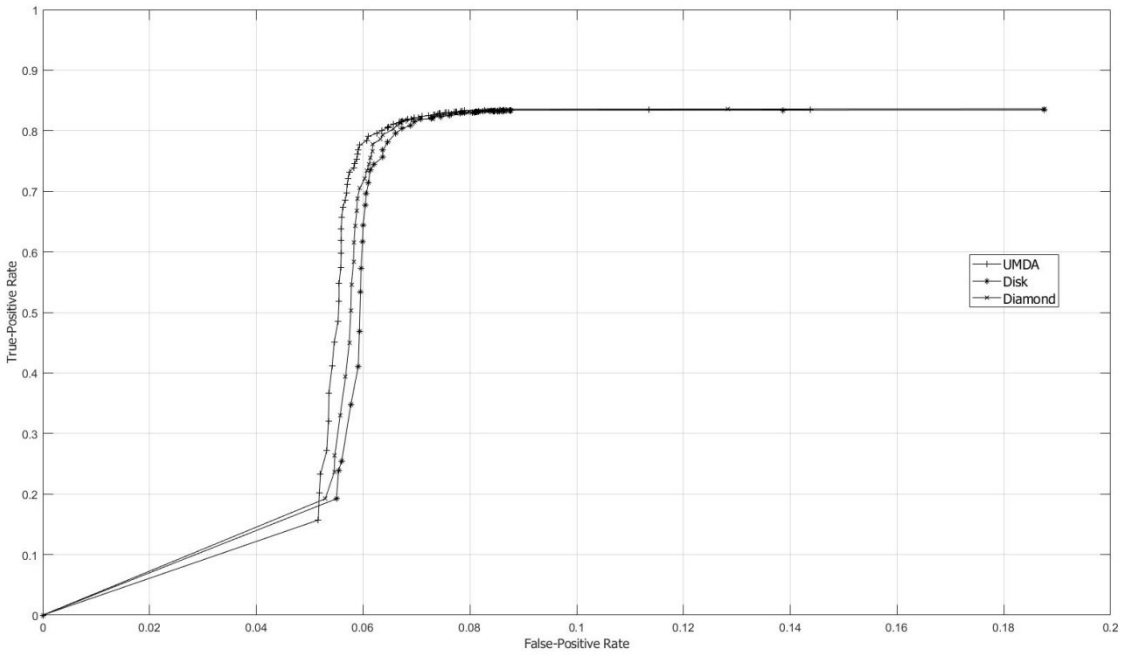

Fig. 6. ROC curves graph using SE sizes from *1x1* to *127x127*. The SE size was the varying parameter used to study the classificatory performance. The FPR and TPR are represented on the *x-axis* and *y-axis*, respectively.

By contrasting Accuracy and ROC performances, the best result was obtained with a SE of 65x65 pixels. Fig. 7 shows a sample of the best SE's achieved by UMDA.

Fig. 7. Best SE achieved by UMDA.

In Fig. 8 the Accuracy comparison between the K-Means algorithm and the top-hat operator with their SE variants is shown.

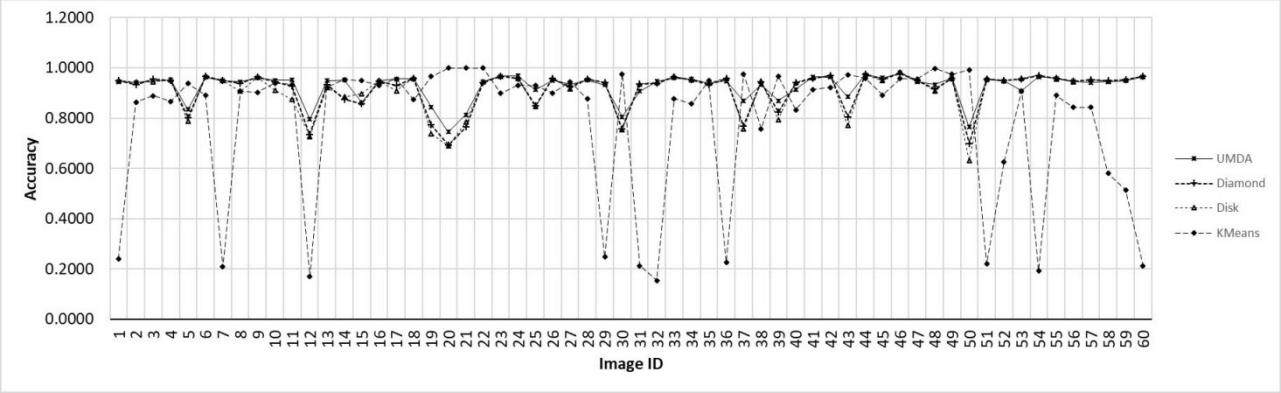

Fig. 8. Accuracy chart for the evaluated methods for each image. The *x-axis* contains each image ID. The *y-axis* contains the best achieved accuracy value by each method.

The Fig. 9 presents the accuracy results separated by each method.

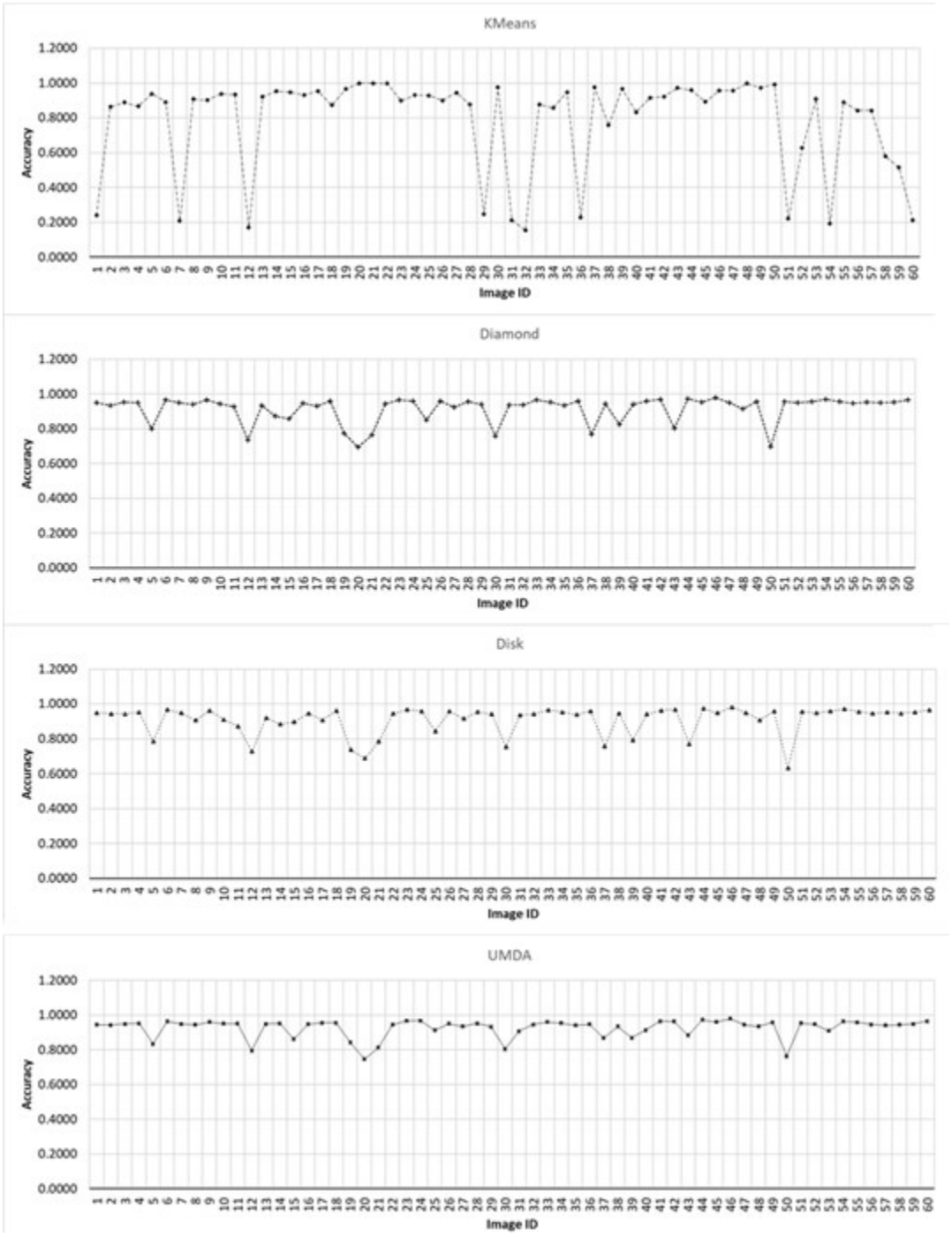

Fig. 9. Accuracy chart of results obtained by each method and image. The *x-axis* contains each image ID. The *y-axis* contains the best achieved accuracy value.

Discussion

After test execution, the best performance was achieved by the top-hat operator using the UMDA generated structuring elements and it was verified contrasting the ROC curve graph with the performance data. Figs. 10 and 11 shows a subset of 5 images with their respective ground-truth and responses by the various methods applied for its segmentation.

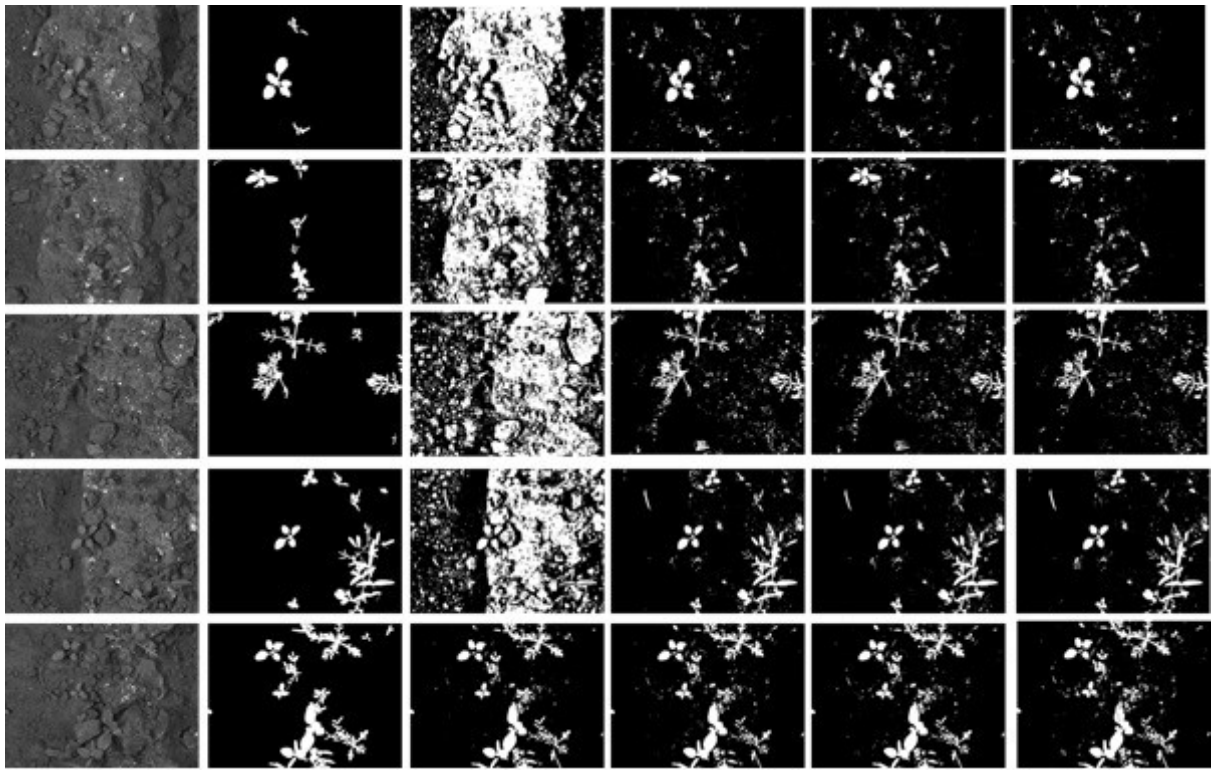

Fig. 10. Subset of segmented images applying the K-Means method and the top-hat operator. From left to right, **first column** shows the original crop image; **second column** shows the ground-truth image; **third column** shows the K-Means segmentation result; **fourth column** shows the top-hat operator response using a disk SE with size of *65x65*; **fifth column** shows the top-hat operator response using a diamond SE with size of *65x65*; **last column** shows the top-hat operator response using the adaptive SE generated by UMDA with size of *65x65*.

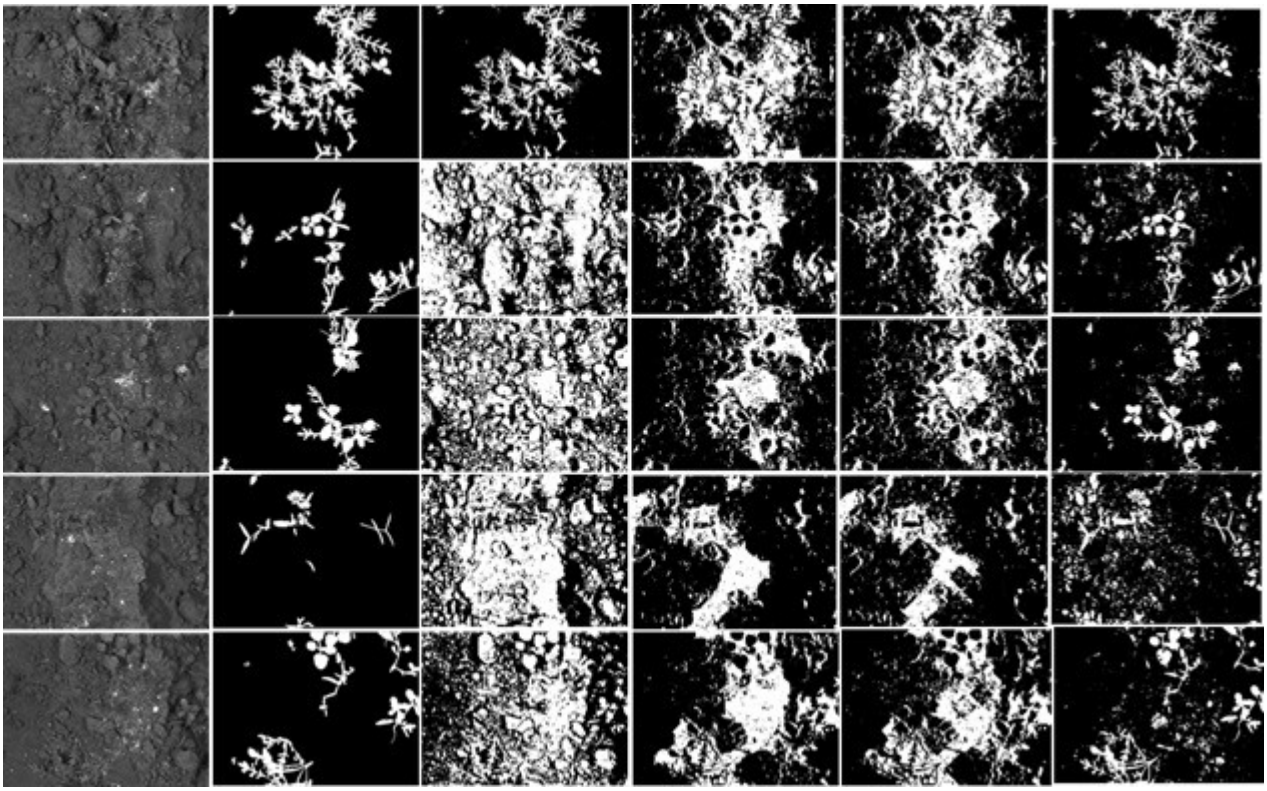

Fig. 11. Subset of segmented images applying the K-Means method and the top-hat operator. From left to right, **first column** shows the original crop image; **second column** shows the ground-truth image; **third column** shows the K-Means segmentation result; **fourth column** shows the top-hat operator response using a disk SE with size of *65x65*; **fifth column** shows the top-hat operator response using a diamond SE with size of *65x65*; **last column** shows the top-hat operator response using the adaptive SE generated by UMDA with size of *65x65*.

The segmentation results achieved by K-Means shows difficulties to segment crop images with low contrast obtaining high rates of false-positives in most of them. The top-hat operator with disk and diamond shapes perform better than K-Means algorithm however, most of crops has an uneven shape and size including a low contrast with the background. For that reason, the adaptive shape improves all performance factors under a certain SE size as presented in Fig. 5. Since white top-hat operator removes objects with less size than the structuring element, the UMDA was able to evaluate multiple combinations of shapes and sizes, selecting the best overall size for the structuring elements. Also, the structuring elements builded by UMDA performs better removing non-crop pixels than classic shapes as it was illustrated in Figs. 10 and 11 in the last column. As presented in Fig. 12, the adaptive SE achieved a better result than rest of techniques because it was able to remove more non-crop pixels in the original image.

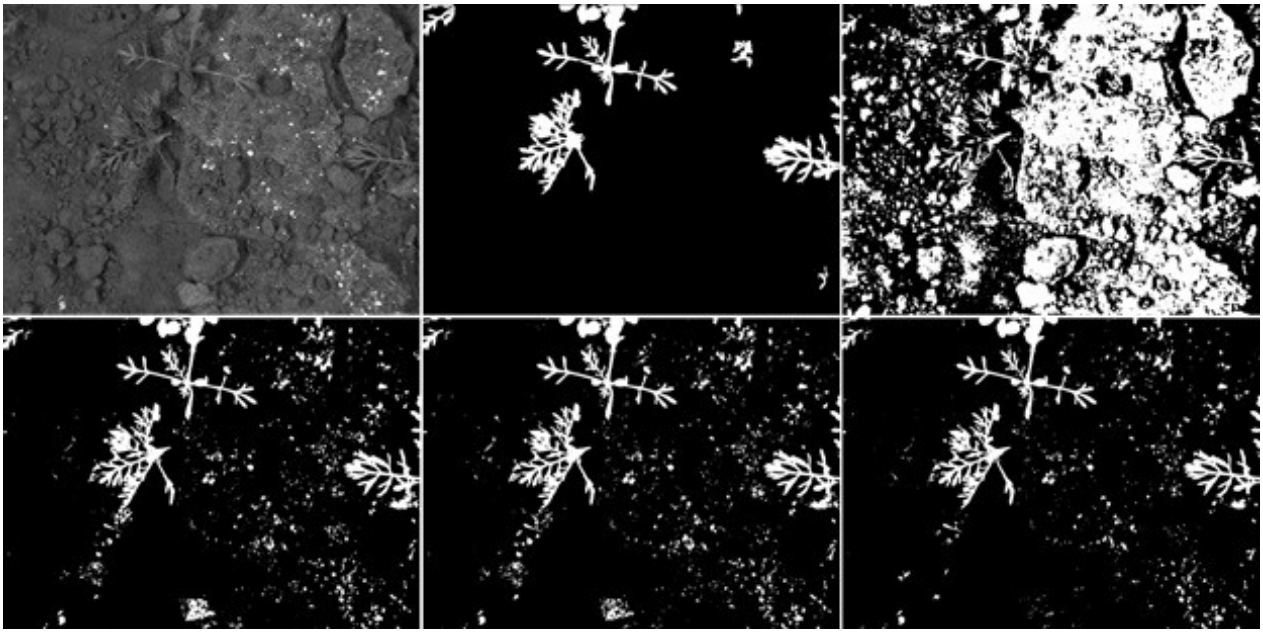

Fig. 12. Example of a crop image with low contrast and its segmentation results. From left to right and up to down: the original crop image; the ground-truth delined by an specialist; the result achieved by K-Means; the result achieved using the top-hat operator with 65x65 disk SE; the result using the top-hat operator with 65x65 diamond SE; the result using the top-hat operator using a 65x65 adaptive SE.

According with ROC curve graph presented in Fig. 5, the adaptive SE appears to achieve better results and, considering the original image resolution that is *1296x966* pixels, the differences with other methods become more significant. Also, the the accuracy performance was contrasted with the ROC curve since considering only the accuracy measure can conduct to wrong results and missinterpretations as described by (Zhu, 2010). For example, one of the highest accuracy performances was achieved using an adaptive SE with size of 1x1. However, making a closer view in data presented at Table 2 and contrasting with ROC curve presented in Fig. 6, the true-positive fraction was very low compared with a SE with size of 65x65 were the true-positive fraction assesses the accuracy factor.

Also, it is important to realize about the SE shapes and their content. For example, disk and diamond SE's are solid shapes unlike those generated by UMDA since it has not restrictions in any way. This means for example, that disk and diamond shapes has not empty regions inside unlike those achieved by UMDA. Due to the presence of empty regions inside of the adaptive SE's the removal or keeping of certain elements inside the image could be done in a wrong way by the processes of erosion and dilation performed by the top-hat operator. This is an important

issue to be addressed and studied on future research works since it could conduct to improve the results by adding shape restrictions to the UMDA. Based on this study, future work will be related to reduce the decay rates by adding constraints to the search strategy in order to overcome current issues and also, as a mean to generate a robust set of structuring elements that could be applied to a wide variety of sizes and sizes of crops into digital images.

Acknowledgments

We want to thank to the Programa para el Desarrollo Profesional Docente (PRODEP) and the Universidad Tecnológica de León for give us all necessary support to perform this research though Project UTLEON-CA-18:IDCA-24193. Also, we express our gratitude to the Universidad de Guanajuato for giving us the required support and assessment.

References

Alba E., Madera J., Dorronsoro B., Ochoa A. and Soto M. (2006). Theory and Practice of Cellular UMDA for Discrete Optimization, 242-251. Parallel Problem Solving from *Nature - PPSN* IX. Vol. 4193. Springer.

Bouraoui B., Ronse C., Baruthio J., Passat N. and Germain P. (2008). Fully automatic 3D segmentation of coronary arteries based on mathematical motphology, 1059-1062. *5th IEEE International Symposium on Biomedical Imaging (ISBI)*. IEEE.

Cruz Aceves I., Hernández Aguirre A. and Aviña Cervantes J.G. (2015). Automatic segmentation of coronary arteries using a multiscale Top-Hat operator and multiobjective optimization, 297-320. *Revista Electrónica Nova Scientia*.

Eiho S. and Qian Y. (1997). Detection of coronary artery tree using morphological operator, 696-699. *Computers in cardiology*. Vol. 24. IEEE.

Frangi A.F., Niessen, W.J., Vincken K.L. and Viergever M.A. (1998). Multiscale vessel enhancement filtering. Medical Image Computing and Computer-Assisted Intervention — *MICCAI'98*. Vol. 1496. Springer.

Guerrero-Turrubiates J.J. Cruz-Aceves I., Ledesma S., Sierra-Hernández J.M., Velasco J., Avina-Cervantes J.G., Avila-Garcia M.S., Rostro-Gonzalez H. and Rojas-Laguna R. (2017). Fast parabola detection using estimation of distribution algorithms, 1-13. *Computational and Mathematical Methods in Medicine*. Hindawi.

Haugh S. and Ostermann J. (2015). *A Crop/Weed Field Image Dataset for the Evaluation of Computer Vision Based Precision Agriculture Tasks*, 105-116. Springer Editorial.

Hauschild M. and Pelikan M. (2011). An introduction and survey of estimation of distribution algorithms, 111-128. *Swarm and Evolutionary Computation*. Vol. 1.

Heinz M. and Mahnig T. (2001). *Evolutionary algorithms: From recombination to search distributions*, 135-173. Springer.

Hisashi H. (2005). Estimation of Distribution Algorithms with Mutation, 112-121. *European Conference on Evolutionary Computation in Combinatorial Optimization*. Springer.

Hu, J., Kashi, R., Lopresti, D., Nagy, G. and Wilfong, G. (2001). Why Table Ground-Truthing is Hard, 129-133. *Proceedings of Sixth International Conference on Document Analysis and Recognition*. IEEE.

Jaware, T., Badgujar R.D. and Patil, G. (2012). Crop Disease Detection using Image Segmentation. *Proceedings of "Conference on Advances in Communication and Computing (NCACC'12)"*, 190-194. India: R.C. Patel Institute of Technology, Shirpur, Dist. Dhule, Maharastra.

Jian-zhuang, L. and Wen-qing, L. (1991). The Automatic threshold of gray level pictures via Two-dimentional Otsu Method, 325-327. *International Conference on Circuits and Systems*. China.

MacQueen J. (1967). *Some Methods for Classification and Analysis of Multivariate Observations*. Fifth Berkeley Symposium. Los Angeles: University of California.

Marler R. T. and Arora J. S. (2010). The weighted sum method for multi-objective optimization: new insights, Struct, 853-862. *Multidiscipl. Optim*. Vol. 41.

Meyer F. (1977). *Contrast feature extraction. Quantitative Analysis of Microstructures in Material Scences, Biology and Medicine*.

Patil R., Udgave S., More S., Nemishte D. and Kasture M. (2016). Grape Leaf Disease Detection Using K-means Clustering Algorithm. *International Research Journal of Engineering and Technology (IRJET)*, 2330-2333. Vol. 3.

Qu, Z. and Hang, L. *Research on Image Segmentation Based on the Improved Otsu Algorithm*. (2010). 2010 Second International Conference on Intelligent Human-Machine Systems and Cybernetics, 228-231. IEEE.

Soille P. (1999). *Morphological Image Analysis: Principles and Applications*. Springer-Verlag Editorial.

Sun K. and Sang, N. (2008). Morphological enhancement of vascular angiogram with multiscale detected by gabor filters. *Electronic letters*. Vol. 4.

Swets J. (1988). Measuring the Accuracy of Diagnostic Systems. *Science* 240(4857), 1285-1293.

Topon Kumar P. and Hitoshi I. (2003). Reinforcement Learning Estimation of Distribution Algorithm, 1259-1270. *Genetic and Evolutionary Computation Conference*. Springer.

Vala, H. and Baxi, A. (2013). *A Review on Otsu Image Segmentation Algorithm*, 387-389. Vol. 2.

Wang S, Li B. and Zhou S. (2012). A Segmentation Method of Coronary Angiograms Based on Multi-scale Filtering and Region-Growing. Conference: *Biomedical Engineering and Biotechnology (iCBEB)*, 2012.

Zhu W., Zeng N. and Wang N. (2010). *Sensitivity, Specificity, Accuracy, Associated Confidence Interval and ROC Analysis with Practical SAS ® Implementations*. NESUG 2010.